Control of Secondary Flow in a Low Solidity Circular Cascade Diffuser

Daisaku Sakaguchi[1], Takuji Fujii[1], Hironobu Ueki[1], Masahiro Ishida[1], and Hiroshi Hayami[2]

1. Nagasaki University 1-14 Bunkyo-machi, Nagasaki, 852-521, Japan
2. Kyushu University (retired)

According to the previous experimental works on the low solidity circular cascade diffuser (LSD), a pressure recovery of a centrifugal blower was improved by the LSD significantly in a wide range of flow rate, and the pressure recovery was improved further by the LSD with a tandem cascade in comparison with the LSD with a single-row cascade. In the present study, the flow behavior in the LSD with the tandem cascade has been analyzed numerically by using the commercial CFD code of ANSYS-CFX12. It was shown clearly that the higher pressure recovery was achieved by applying the LSD with the tandem cascade, and the high pressure recovery is based on the high pressure rise in the vaneless space upstream of the LSD and the high blade loading of the front blade of the LSD. The high pressure recovery in the LSD could be achieved by controlling the flow separation on the suction surface of the front blade and also on that of the rear blade due to formation of the favorable secondary flow and due to increase in mass flow passing through the slit section between the front and rear blades.

Keywords: LSD (Low solidity circular cascade diffuser), Centrifugal blower, Range enhancement, Tandem cascade

Introduction

A high pressure ratio and a wide operating range are required in recent centrifugal compressors and blowers. If the impeller tip speed increases, a high pressure ratio can be achieved, but a large dynamic pressure at the impeller exit results. In such a case, a high performance diffuser, for instance, a low solidity circular cascade diffuser (LSD) is essential, which has been widely used in many centrifugal blowers [1,2,3] and compressors [4,5]. The LSD showed a high blade loading without stall even under low flow rate conditions, showing fairly high lift coefficients because the flow separation on suction surface of the LSD blade was successfully suppressed by the secondary flow formed along the side walls. The secondary flow was a reverse flow toward the impeller exit from the rear part of the LSD blade, and the low energy fluid in the reverse flow was regenerated by merging with the main flow discharged from the impeller exit.

The authors [6,7] proposed the LSD with a small tip-groove located at the leading edge of the LSD blade as one of the devices which could control the secondary flow. A high LSD performance was achieved at small flow rates by formations of the stable vortex in the shroud tip-groove and the secondary flow moving circumferentially along the shroud wall toward the impeller exit. It was found that the optimized tip-groove configuration was very effective for formation of the favorable secondary flow in the case of the LSD with a single-row cascade.

A tandem cascade acted as a more effective device for improvement in the LSD performance. Senoo et al. [1] showed the advantage of the LSD with a tandem cascade in a low-speed centrifugal blower. The front blade-row of the tandem cascade was designed suitably for small flow rates while the rear blade-row of the cascade was designed suitably for large flow rate so that the tandem cascade could achieve a high pressure recovery in a wide

range of flow rate. In the present study, the internal flow in the LSD with a tandem cascade is analyzed numerically by using the commercial CFD code of ANSYS-CFX12, in which the secondary flow behavior is compared between the cases with a single-row cascade and a tandem one, and it is clarified the reason why the pressure recovery is improved more by the LSD with a tandem cascade.

Experiment and Numerical Simulation

The test facility was specially designed to keep an axisymmetric flow field in the present experimental work. The test impeller is a low specific speed type open shrouded centrifugal impeller for industrial use, and it has the exit diameter of 510 mm and 16 backward leaning blades with the exit blade angle of 45 deg. The exit blade height is 17.0 mm, and the axial clearance between the impeller shroud tip and the shroud casing wall is 1.0 mm. The air was discharged axisymmetrically to the atmosphere from the diffuser exit with its radius ratio of about 1.6. In the experimental study, the impeller was operated at a constant speed of 2,000±2 rev/min. The static pressures were measured by means of manometers at the suction plenum tank located upstream of the suction pipe and at the impeller exit R=1.0 on the shroud wall. The flow rate was measured by using the entrance nozzle at the inlet of suction pipe.

Figure 2 shows location and shape of the LSD blade in the four cases with the single-row cascade and the tandem cascade. The U.S.A. 35-B airfoil is adopted as the LSD blade. In the case of the single-row cascade as shown in Fig.2 (a), the number of the LSD blade is 11, the solidity of the cascade is 0.693 and the leading edge of the LSD blade is located at the radius ratio of R=1.10 downstream of the impeller exit. Fig.2 (b) shows the case

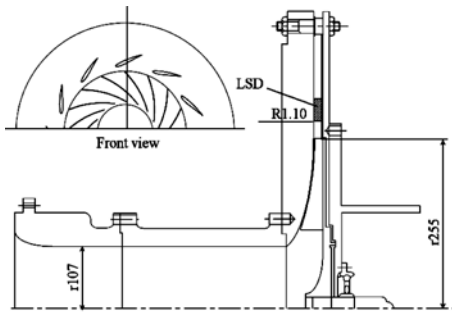

Fig.1 Meridional section of test blower

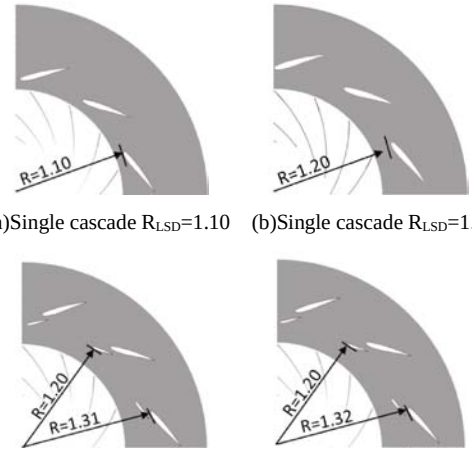

(a)Single cascade R_{LSD}=1.10 (b)Single cascade R_{LSD}=1.20

(c) Tandem cascade R_{rear}=1.31 (d) Tandem cascade R_{rear}=1.32

Fig.2 Configuration of LSD

of the single-row cascade with the leading edge located at R=1.20. In the cases of the single-row cascade, the stagger angle of the LSD blade is 66 deg, which is equal to the mean absolute flow angle at the impeller exit under the design flow rate of ϕ_d=0.27. In the cases of the tandem cascade shown in Figs.2 (c) and (d), the configurations of the front and rear blade rows were referred in the previous work [8]. The number of blade is 11, and the overlapping of the front and rear blades is 9% of the blade pitch. The stagger angle of the front blade is 72 deg, which corresponds to the flow angle at the small flow rate. The solidity of the front blade is 0.315 and the leading edge is located at R=1.20. The stagger angle of the rear blade is 58 deg, which corresponds to the flow angle at the large flow rate. The effect of the slit width between the front and rear blades was investigated by changing the leading edge position of the rear blade from R_{rear}= 1.31 to 1.32 as shown in Figs. 2(c) and (d). The solidity of the rear blade is 0.600 in the case of R_{rear}=1.31 and is 0.596 in the case of R_{rear}=1.32.

The 3-D turbulent internal flow was calculated by using the commercial CFD code of ANSYS-CFX12 together with the baseline *k-ω* turbulence model. The multi-frame of references consisting of the rotating domain of the impeller section and the stationary domain of the diffuser section were adopted. In the steady flow analysis, one of the impeller passages and one of the LSD passages were selected and the periodic boundary condition was applied at the mid-pitch of the blade passage. The grid number is about 130,000 for the rotating domain and about 550,000 for the stationary domain. The domain interface between the rotating frame and the stationary frame was located at R=1.01 in the vaneless space shown as a red region in Fig.3. Then, non-uniformity of the circumferential flow distortion at the upstream exit boundary of the domain interface was not retained at the downstream inlet boundary although the flow distortion in the

meridional plane was conserved at the interface.

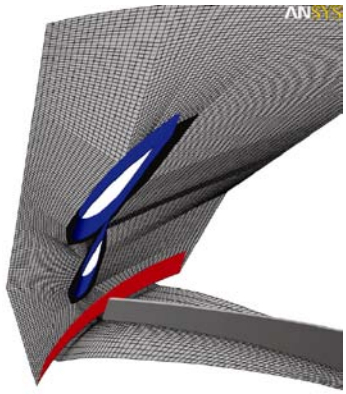

Fig. 3 Computational grid

Results and Discussions

Characteristics of test blower

The characteristics of the test blower are compared between the experimental results and the numerical simulation results in Fig.4. The abscissa is the discharged flow coefficient ϕ, the left ordinate is the static pressure coefficient, and the right ordinate is the total to static efficiency $\eta_{t\text{-}s}$. In the figure, ψ_{s2} denotes the static pressure coefficient at the impeller exit and ψ_{se} is the one at the diffuser exit. The numerical results in both cases of the vaneless diffuser and the LSD with the single-row cascade agree well with the experimental results within the experimental accuracy, which means that the simulation grid and the turbulence model adopted in the simulation are quite valid.

The experimental results show clearly that the static pressure coefficient at the diffuser exit ψ_{se} and the total to static efficiency are improved by the LSD in the wide flow rate range, in addition, the inception flow rate of diffuser stall is successfully decreased to the smaller flow rate by about 10% as shown by the solid circle marks in Fig.4. It is found that the LSD is effective not only for improving the pressure rise but also for enhancing the flow rate range.

The predicted pressure coefficients are compared between several cases with different types of LSD in Fig.5. In the figure, ψ_d is the static pressure rise in the diffuser stage calculated by $\psi_d=\psi_{se}-\psi_{s2}$. With respect to the LSD with the single-row cascade, ψ_d shows higher in the case of R_{LSD}=1.20 than that of R_{LSD}=1.10 at small flow rates. With respect to the LSD with the tandem cascade, ψ_d is improved in the wide flow rate range in comparison with the single-row cascade cases, and it is higher in the case of R_{rear}=1.32 than that of R_{rear}=1.31 at small flow rates. Comparing between the LSDs with the tandem cascade and the single-row cascade, the static pressure coefficient at the diffuser exit was improved by 2% at the design flow rate and by 4% at the small flow rate.

Pressure recovery in diffuser

The pressure distribution in the diffuser between the impeller exit and the diffuser exit is compared in Fig.6. The ordinate is the pressure recovery evaluated by the following equation;

$$C_{PR} = \frac{p_i - p_2}{0.5 \cdot \rho_2 \cdot V_2^2} \qquad (1)$$

where p_i denotes the averaged static pressure at the radial position i, p_2 is the static pressure averaged at the impeller exit section, ρ is the fluid density and V_2 is the mean absolute velocity at the impeller exit.

In the case of the vaneless diffuser, the mean dynamic pressure at the impeller exit is converted into the static pressure by only about 40% until the diffuser exit. On the other hand, in the case of the tandem cascade, 60% of the dynamic pressure is successfully converted.

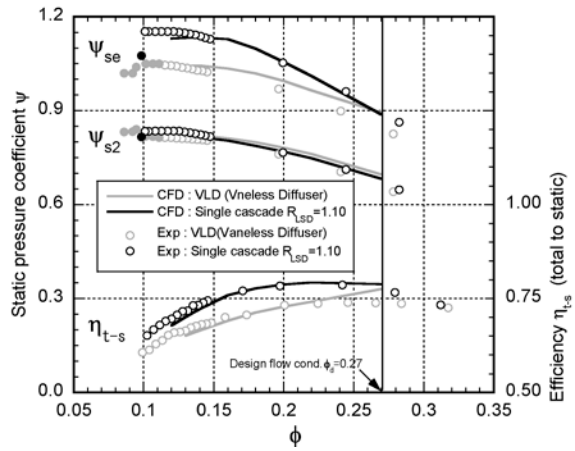

Fig. 4 Comparison of blower characteristics between experiment and numerical simulation

With respect to the pressure recovery in the vaneless space between R=1.0 to 1.10, it is the maximum in the case of the vaneless diffuser and it is the minimum in that of the single-row cascade with the leading edge of R_{LSD}=1.10. In the case of the single-row cascade with R_{LSD}=1.20, the pressure recovery in the vaneless space is almost equal to the one of the vaneless diffuser. The maximum pressure recovery in the vaneless space between R=1.0 to 1.2 is achieved in the cases with the tandem cascade; 33% of the total pressure recovery in the diffuser is obtained in the vaneless space and 50% of the one is obtained in the front blade-row. The extremely high pressure recovery is achieved by adopting the front

blade-row with very low solidity of 0.315, and by increasing the slit width between the front blade and the rear blade moving the leading edge of the rear blade from R_{rear}=1.31 to 1.32.

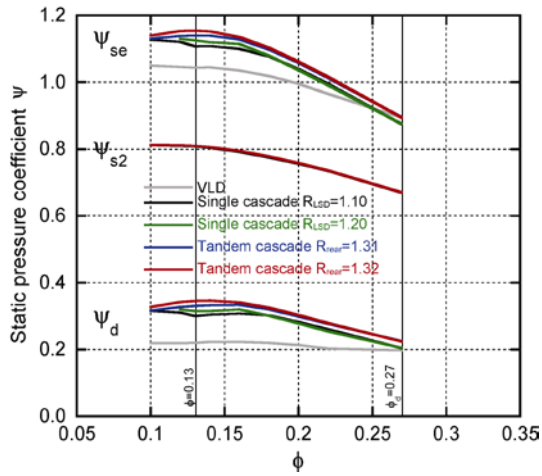

Fig. 5 Comparison of predicted pressure coefficient

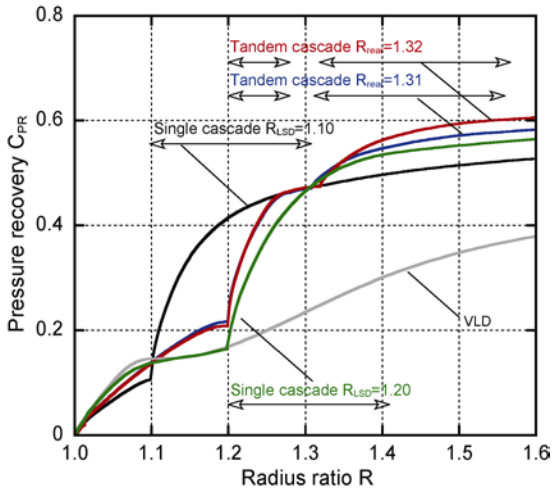

Fig. 6 Comparison of pressure recovery C_{PR} (ϕ=0.13)

Velocity distribution in diffuser

In order to clarify the mechanism of the high pressure recovery due to the LSD, the meridional velocity distributions are compared in Fig.7 between four cases with the single-row cascade and the tandem cascade in the case of the low flow rate of ϕ=0.13, where the radial component of velocity is averaged circumferentially as the mass-weighted value.

In the case of the single-row cascade with the leading edge of R_{LSD}=1.10, the discharged flow from the impeller exit is accelerated in the vaneless space between R=1.0 and 1.10 because of formation of the reverse flow zone on the shroud side wall. Downstream of the vaneless space, the high velocity region moves from the hub side to the shroud side, as was seen in the literatures [9,10]. In the case of the single-row cascade with R_{LSD}= 1.20, the large reverse flow zone is formed on the hub side wall, and the main flow is accelerated remarkably at the shroud side. As shown in Fig.6, the deteriorated pressure rise in the vaneless space between R=1.1 to 1.2 is due to the large reverse flow zone at the hub side.

On the other hand, in the cases of the tandem cascade with R_{LSD}=1.20, the reverse flow zone remains at the shroud side throughout the diffuser from the impeller exit until downstream of the rear blade of the cascade, and it is thinner compared with the case of the single-row cascade. It is, then, reasonable that the pressure recovery in the vaneless space is higher in the cases of the tandem cascade than in case of the single-row cascade with R_{LSD}=1.20 as shown in Fig.6.

Figures 8(a) and (b) show the velocity distributions between shroud and hub at the radius ratio of R=1.05; Fig.8(a) shows the radial component and Fig.8(b) shows the circumferential component. The distributions of radial component of velocity are almost similar occupying the reverse flow zone about 10% of the diffuser depth except for the case of the single-row cascade with R_{LSD}= 1.20. With respect to the velocity distributions of circumferential component, in the case of the single-row cascade with R_{LSD}=1.10, it is reduced remarkably at the shroud side, then, that is another reason why the pressure rise in the vaneless space is small as shown by the black solid line in Fig.6. It seems that, in the case of the single-row cascade with R_{LSD}=1.10, the fluid having a small circumferential component decreased by the LSD reverses toward the impeller exit along the shroud wall. In other words, the leading edge of the LSD blade, which is too close to the impeller exit, affects significantly on the pressure recovery in the vaneless space. On the other hand, in the cases of the tandem cascade with R_{LSD}=1.20, the circumferential component of the reverse flow along the shroud wall is little affected by the LSD showing almost the same as the one of the vaneless diffuser. This is why the high pressure recovery in the vaneless space is achieved in the cases of the tandem cascade.

Secondary flow behavior and lift characteristics

With respect to the cases of the tandem cascade, the spatial distributions of reverse flow zone on the diffuser shroud wall and on the suction surface of the front and rear blades are shown in Figs.9(a) and (b) and Figs.10(a) and (b), in which the reverse flow zone is indicated by the blue colored area. Figure 9 is the case of R_{rear}=1.31 and Fig.10 is the case of R_{rear}=1.32. At the front blade of the tandem cascade, the low energy fluid on the suction

surface at the shroud side is accumulated in the rear part of the blade and moves toward the leading edge of the neighboring blade, resulting in formation of the secondary flow. On the other hand, at the rear blade, the separated flow on the suction surface of the blade flows out downstream. It should be noticed that the reverse flow zone of the suction surface of the rear blade is smaller in the case of R_{rear}=1.32 than in that of R_{rear}=1.31.

Figure 11 shows a comparison of the lift characteristics of the rear blade. The lift force was normalized by the average dynamic pressure using the vector average velocity calculated at the two sections; 5 mm upstream and 5 mm downstream of the rear blade respectively. The abscissa is the angle of attack calculated from the discharged flow rate. The lift coefficient increases as the flow rate decreases. The maximum lift coefficient of 1.1 is attained at the small flow rate of ϕ=0.16 in the case of R_{rear}=1.31, on the other hand, the higher maximum lift of 1.3 is attained in the case of R_{rear}=1.32 at the smaller flow rate of ϕ=0.14.

Figures 12(a) and (b) show the representative limiting streamlines on the shroud wall which passes through the slit section between the front and rear blades. The reverse flow zone on the shroud wall is also indicated in the figures. The low energy fluid flowing out from the front blade moves circumferentially along the shroud wall toward the leading edge of the neighboring blade as mentioned in the preceding section. The inception point of flow separation on the suction surface of the rear blade appears farther downstream in the case of R_{rear}=1.32 in comparison with the case of R_{rear}=1.31, resulting in the higher blade loading of the rear blade. This might be due to a difference in the deceleration rate of the slit flow; the deceleration rate in the case of R_{rear}=1.32 seems to be smaller than in that of R_{rear}=1.31.

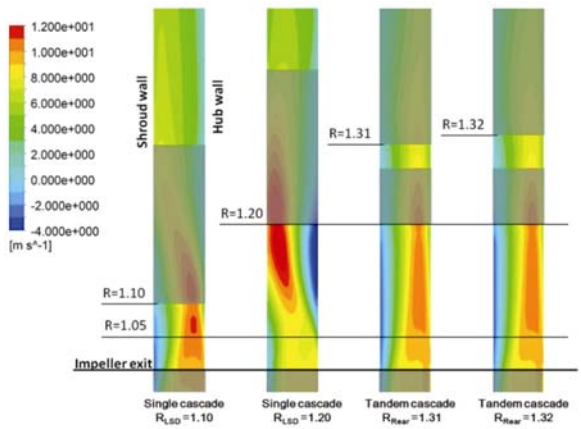

Fig. 7 Radial velocity contour in meridional plane (ϕ=0.13)

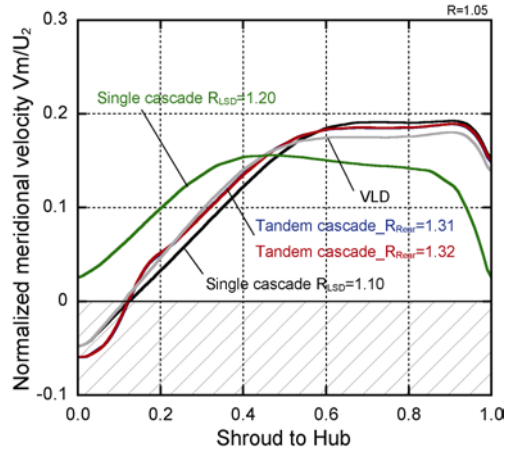

(a) Radial component of velocity

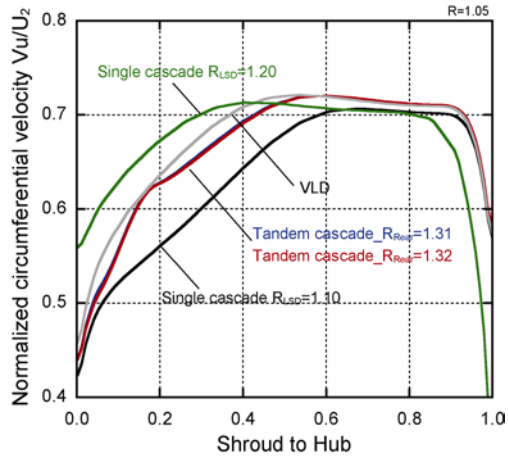

(b) Circumferential component of velocity

Fig. 8 Velocity distribution between shroud and hub (R= 1.05, ϕ=0.13)

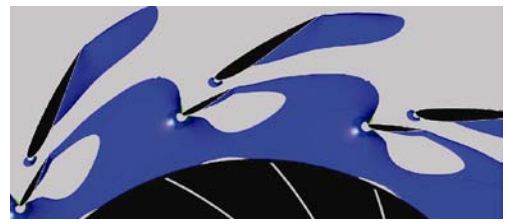

(a) Reverse flow zone on shroud wall

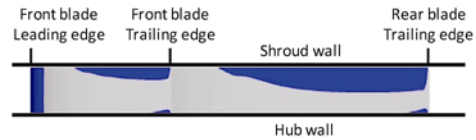

(b) Reverse flow zone on suction surface of LSD blade

Fig. 9 Reverse flow zones on diffuser wall and blade suction surface (Tandem with R_{rear}=1.31, ϕ=0.13)

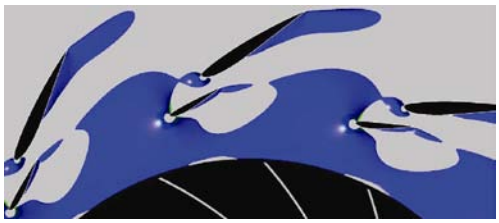

(a) Reverse flow zone on shroud wall

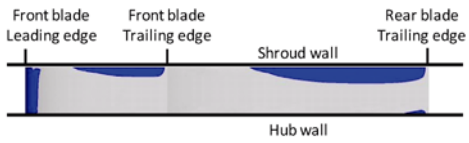

(b) Reverse flow zone on suction surface of LSD Blade

Fig.10 Reverse flow zone on diffuser wall and blade suction surface (Tandem with R_{rear}=1.32, ϕ=0.13)

Figure 13 shows the calculated mass flow rate which passes through the slit section. The mass flow rate between the slit is normalized by the discharged mass flow rate between blades. The ratio of the mass flow rates increases as the discharged flow rate decreases. It is noticed that, in the case of R_{rear}=1.32, the mass flow rate through the slit is larger than in that of R_{rear}=1.31. The maximum flow rate through the slit reaches to 40% of the discharged flow rate at the small flow rate.

It is convinced that, in the case of the tandem cascade, the high pressure recovery of the diffuser is achieved by three factors, that is, the pressure rise in the vaneless space due to locating the leading edge of the LSD at R_{LSD}=1.20 relatively far from the impeller exit, the high blade loading at the front blade due to formation of the favorable secondary flow, and the suppression of separation on the suction surface of the rear blade due to the increased mass flow through the slit.

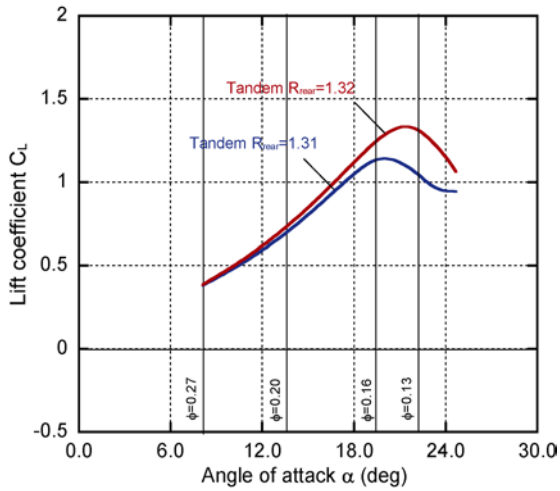

Fig.11 Lift characteristics of rear blade

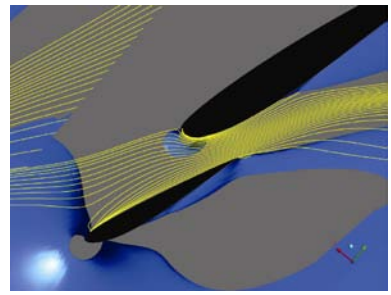

(a) Tandem cascade with R_{rear}=1.31

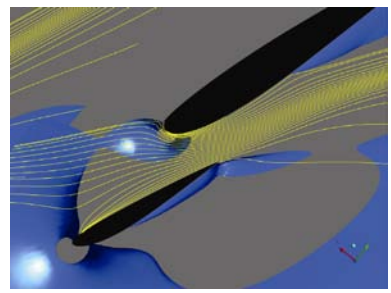

(b) Tandem cascade with R_{rear}=1.32

Fig.12 Reverse flow zone and limiting streamline on shroud wall (ϕ=0.13)

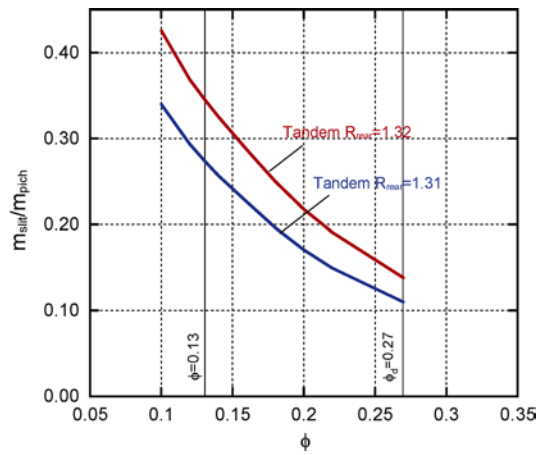

Fig.13 Comparison of mass flow rate passing through slit section

Conclusions

The high pressure recovery of the low solidity diffuser with the tandem cascade was investigated in view point of the secondary flow analyzing the flow behavior in the diffuser based on the three dimensional numerical simulation. It is clarified that, in the case of the tandem cascade, the high pressure recovery of the diffuser is achieved by the following three factors.

The high pressure rise in the vaneless space is

achieved by locating the leading edge of the front blade relatively far from the impeller exit,

The high blade loading of the front blade is achieved by formation of the favorable secondary flow which suppresses the flow separation on the suction surface of the front blade.

The flow separation on the suction surface of the rear blade is suppressed by increasing the mass flow passing through the slit section between the front and rear blades.

Acknowledgements

This work was financially supported by the Harada Memorial Foundation, and the authors also would like to thank to graduate students of Energy System Laboratory, Nagasaki University.

References

[1] Senoo, Y., Hayami, H. and Ueki, H., (1983) Low-Solidity Tandem-Cascade Diffusers for Wide-Flow-Range Centrifugal Blowers, Phoenix, AZ, USA, ASME paper No.83-GT-3 pp.1–7

[2] Senoo, Y., Kawano, M. and Hayami, H., (1979) A Low Solidity Cascade Diffuser, Transactions of the Japan Society of Mechanical Engineers, Series B, Vol.45, No.396 pp.1099–1107 (In Japanese)

[3] Senoo, Y., Hayami, H. and Ueki, H., (1986) Low-solidity Cascade Diffusers for Wide-flow-range Centrifugal Blowers, International Journal of Turbo and Jet Engines, Volume 3, pp.33-41

[4] Hayami, H., Senoo, Y. and Utsunomiya, K., (1990) Application of low-solidity cascade diffuser to transonic centrifugal compressor, Tranactions of the ASME, Journal of Turbomachinery, Vol.112-1, pp.25–29

[5] Tamaki, H., (2000) Study on Optimization of Low Solidity Diffuser, Journal of the Gas Turbine Society of Japan, Vol.28-3, pp.231–237 (In Japanese)

[6] Sakaguchi, D., Ishida, M., Ueki, H.,Hayami, H. and Senoo, Y., (2008) Analysis of Noise Generated by Low Solidity Cascade Diffuser in a Centrifugal Blower, Berlin, Germany, ASME GT2008-50750

[7] Ishida, M., Murakami, T., Sakaguchi, D., Ueki, H., Hayami, H. and Senoo, Y., (2010) Analysis of Secondary Flow Behavior in Low Solidity Cascade Diffuser of a Centrifugal Blower, Glasgow, Scotland, UK, ASME GT2010-2861

[8] Hayami, H., Senoo, Y., Kitayama, F., (1985) Correction of Lift Coefficient for Tandem Circular-Cascade Diffusers, Bulletin of the JSME, Vol.28-241, pp. 1354–1358

[9] Senoo, Y., Kinoshita, Y. and Ishida, M., (1977) Asymmetric Flow in Vaneless Diffusers of Centrifugal Blowers, Transactions of the ASME, Journal of Fluids Engineering, Vol.99-1, pp.104–114

[10] Ishida, M., Sakaguchi, D., Sun, Z. and Ueki, H., (2004) Computational Analysis of 3-D Turbulent Flow Separation in a Vaneless Diffuser (in Japanese), Transactions of the Japan Society of Mechanical Engineers Series B, Vol.70–691, pp.623–628